Available online at www.sciencedirect.com
ScienceDirect
Trans. Nonferrous Met. Soc. China 26(2016) 1482−1490
Transactions of Nonferrous Metals Society of China
www.tnmsc.cn

Effect of pre-deformation on microstructures and mechanical properties of high purity Al−Cu−Mg alloy

Hui-zhong LI[1,2,3], Ruo-mei LIU[1], Xiao-peng LIANG[1,2], Min DENG[1], Hui-juan LIAO[1], Lan HUANG[2]

1. School of Materials Science and Engineering, Central South University, Changsha 410083, China;
2. State Key Laboratory of Powder Metallurgy, Central South University, Changsha 410083, China;
3. Key Laboratory of Nonferrous Metal Materials Science and Engineering, Ministry of Education, Central South University, Changsha 410083, China

Received 18 April 2015; accepted 11 April 2016

Abstract: The effects of pre-deformation following solution treatment on the microstructure and mechanical properties of aged high purity Al−Cu−Mg alloy were studied by tensile test, micro-hardness measurements, transmission electron microscopy and scanning electron microscopy. The micro-hardness measurements indicate that compared with un-deformed samples, the peak hardness is increased and the time to reach peak hardness is reduced with increasing pre-strain. Additionally, a double-peak hardness evolution behavior of cold-rolled (CR) samples was observed during aging. The results of TEM observation show that the number density of S'(Al_2CuMg) phase is increased and the size is decreased in CR alloy with increase of pre-strain. The peak hardness and peak strength of the CR alloy are increased because of quantity increasing and refinement of S' phase and high density dislocation.
Key words: Al−Cu−Mg alloy; pre-deformation; age strengthening; precipitation; microstructure; mechanical properties

1 Introduction

Heat-treatable aluminum alloys belonging to Al−Cu−Mg system are required for many structural applications, especially in the aerospace industry due to their attractive mechanical properties [1−3]. The Al−Cu−Mg alloys dated from the discovery of the age-hardening phenomenon [4]. For the last 100 years, excellent specific strength, formability and corrosion resistance have made age-hardenable Al−Cu−Mg alloys attractive candidates for a number of applications [3−6]. Generally, the high performance mechanical properties of this kind of alloy can be achieved by thermo-mechanical treatment (TMT) process, which can provide the excellent performance of material by taking advantage of its deformation strengthening during plastic deformation and the transformation strengthening during heat treatment [7,8]. QUAN et al [9] indicated that the pre-deformation can increase the strength and reduce the time to reach the peak hardness of 2524 Al alloy. NING et al [10] studied the effect of cold deformation on characteristics of 2024 Al alloy and found that a characteristic of double peaks aging strengthening phenomenon appears. A high density of dislocation introduced by cold deformation accelerates the precipitation of GP zones and aging response of the alloy. It is reported that finer and thinner S'' phase can be obtained in Al−4.45Cu−1.5Mg alloy by cold rolling with a reduction of 40% followed by aging [11]. In addition, the effect of pre-stretching on the precipitation process in other alloys was also studied [12−14]. ZHAO et al [15] reported that simultaneous high strength and ductility were achieved in cold-worked 2024 Al alloy after artificial aging. REN et al [16] showed that high strength and good ductility of 2E12 alloy can be achieved simultaneously by means of TMT. Despite of these reports, there has been no detailed microstructure analysis reported on the mechanism of the effect of pre-deformation on the high purity Al−Cu−Mg alloy.

The aim of this work is to present the effect of various cold-rolling strains on the aging hardening response, microstructure and mechanical properties of the high purity Al−Cu−Mg alloy.

Foundation item: Project (51301209) supported by the National Natural Science Foundation of China
Corresponding author: Xiao-peng LIANG; Tel: +86-731-88830377; Fax: +86-731-88830257; E-mail: liangxp@csu.edu.cn
DOI: 10.1016/S1003-6326(16)64253-X

2 Experimental

The nominal composition of the high purity Al−Cu−Mg alloy is given in Table 1. Solid solution treatment was carried out at 773 K for 3 h, and then the materials were immediately water-quenched to room temperature. Such samples are referred to as the solid-solution-treated (SST) samples hereafter. After SST, cold rolling (CR) was performed at room temperature, reducing the thickness from 2.7 mm to different thicknesses. The rolling reductions ($\varepsilon_r=(t_0-t)/t_0$, where t_0 and t are the thicknesses before and after rolling, respectively) were 10%, 20%, 30% and 40%, respectively, with 5% for each rolling pass. All the specimens were then artificially aged at 453 K for various time.

Subsequently, Vickers micro-hardness and tensile tests were carried out to evaluate the strength and ductility of the samples. Micro-hardness was measured using a pyramid diamond indenter to track the evolution of age hardening, by imposing a load of 4.9 N for 15 s. Specimens ground and polished for tensile testing were dog-bone shaped sheets with a gauge length of 50 mm and a thickness of 2 mm. Tensile tests were carried out at room temperature on a material testing machine (WDW−100A) with a loading rate of 1 mm/min. The strength and ductility were taken from an average of three specimens. The yield strength (YS) was estimated by the stress at 0.2% plastic strain.

Thin foil samples for transmission electron microscopy (TEM) investigations were prepared by cutting, grinding and punching into discs of 3 mm, followed by electro-polishing in a twin-jet Tenupol by solution of 25% nitric acid + 75% methanol at 13.8 V. The microstructure observation was conducted by using an FEI Tecnai $G^2$20 TEM operated at 200 kV.

Table 1 Chemical composition of high purity Al−Cu−Mg alloy (mass fraction, %)

Cu	Mg	Mn	Ti	Zn	Fe	Si	Cr	Al
4.8	1.5	0.4	0.06	0.1	<0.06	<0.06	0.05	Bal.

3 Results

3.1 Mechanical properties

Vickers micro-hardness as a function of aging time for material subjected to different treatments is shown graphically in Fig. 1. The hardness of the SST sample increases gradually to a peak of HV ~152 at 367 min, and then it decreases with longer aging time, indicating the occurrence of over-aging. Obviously, double-peak aging strengthening is achieved in CR-processed samples. Hardness values of all the CR samples are higher than those of the SST samples. The sample with ε_r=10% reaches peak hardness after 300 min aging, which is about 1 h earlier as compared with the SST sample. Subsequently, it softens slightly with prolonged aging time, thereafter the hardness starts to increase again and reaches the second peak hardness after 577 min aging. In contrast, the sample with ε_r=10% and the other three samples with higher ε_r have similar hardness variation trend upon aging. It is clear that the pre-deformation reduces the time to reach peak hardness and improves hardness of the material.

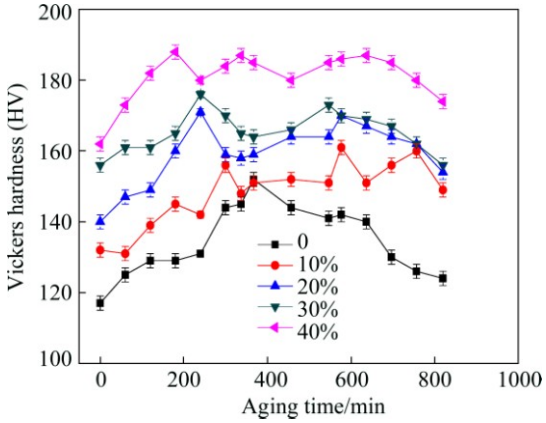

Fig. 1 Evolution of Vickers micro-hardness of alloys subjected to different treatments aged at 453 K for different time

Based on the micro-hardness measurements, tensile tests were performed in order to better understand the mechanical properties of the samples with and without pre-deformation. Figure 2 displays pre-deformation effect on the mechanical properties of test specimen in peak-aged conditions. The matching between micro-hardness and YS indicates that results are in good correlation. As shown, significant strengthening was manifested after cold-rolling, and the ultimate tensile strength (UTS) and YS increase with increasing pre-strain. The UTS, YS and elongation of failure (El) of the SST samples are 431.2 MPa, 373.2 MPa and 21.9%,

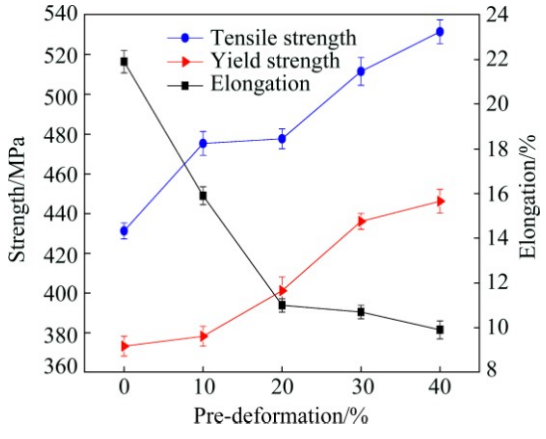

Fig. 2 Mechanical properties of alloy with pre-deformation

respectively. The sample with ε_r=10% has a higher strength than the SST sample. A similar increase in strength is observed in the other CR materials rolled at different levels, while the El of CR samples decreases with increasing pre-strain. Interestingly, the samples with ε_r=40% has the simultaneous high strength (UTS= 531.4 MPa) and respectable ductility (El=9.9%). The El decreases obviously when the alloy is subjected to 10% pre-deformation, then changes very little when the ε_r exceeds 20%, the relatively low elongation about 11% almost remains constant as pre-strain increases, shaping a plateau in elongation curve. The results are in good correlation with those published by HORITA et al [17].

3.2 Tensile fracture morphology

Figure 3 shows the SEM images of tensile fracture morphologies of the material subjected to different levels of pre-deformation. The SST sample presents typical ductile fracture features with many large dimples (Fig. 3(a)), consisting of more dimples than the other alloys. In addition, the coarse dimples containing secondary constituent particles that acted as microcrack precursors are observed. With increasing pre-deformation, the dimple diameter decreases, while the amount of intergranular cleavage increases. For sample, with ε_r=10% (Fig. 3(b)), there are many fine dimples and a small portion of large dimples on fracture surface, showing transgranular and intergranular fracture. By contrast, fracture surface of sample with ε_r=20% is composed of fewer and finer dimples, meanwhile, the depth of dimple is much shallower and its distribution is more heterogeneous (Fig. 3(c)). In samples with ε_r=30% and above, the similar observation is found from Figs. 3(d) and (e). This fracture behavior is consistent with the curve of Fig. 2.

3.3 Microstructure of pre-deformed Al−Cu−Mg alloy

Figure 4 displays the optical images of the alloy subjected to different levels of pre-deformation. As depicted, the grains of samples under different conditions are flat and elongated, paralleling to the rolling direction (RD), illustrating a typical deformed structure.

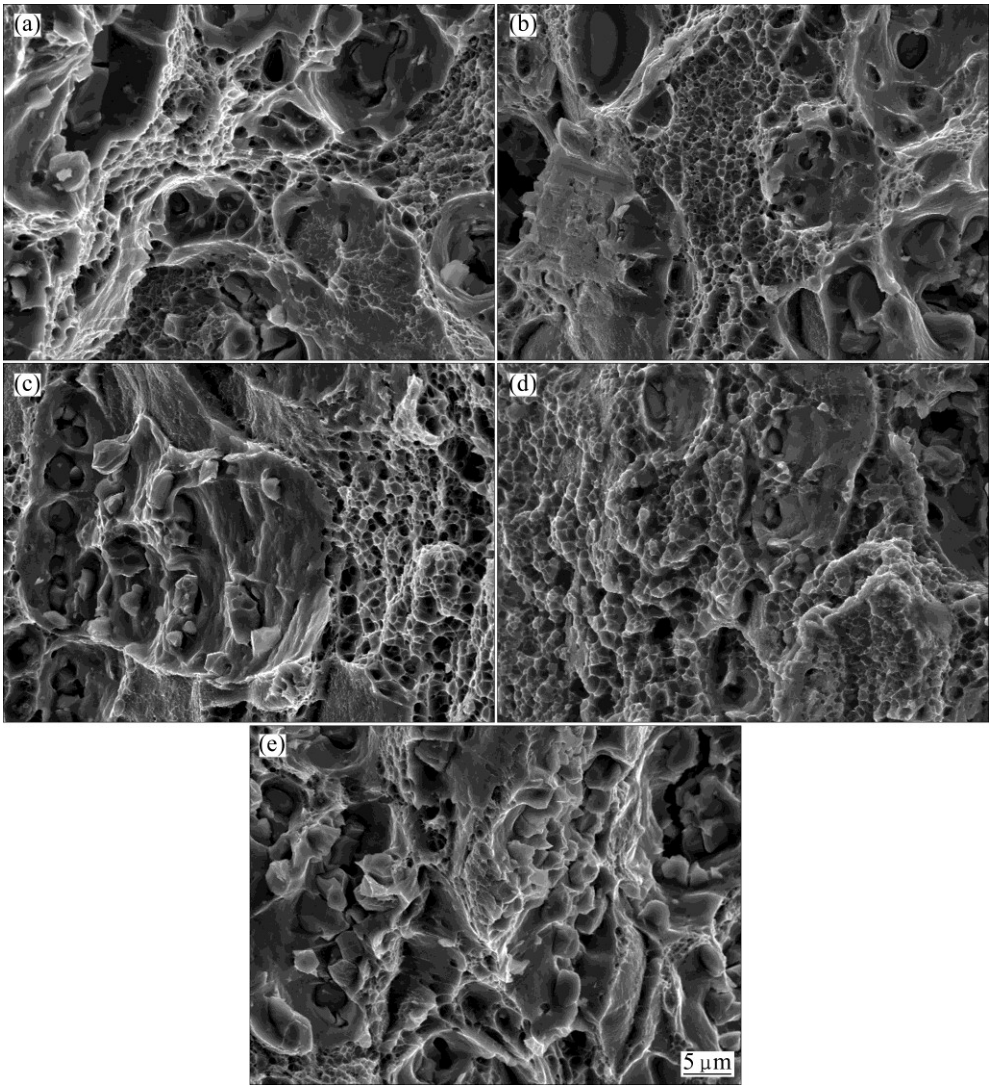

Fig. 3 Tensile fracture morphologies of peak-aged specimen subjected to different ε_r: (a) 0; (b) 10%; (c) 20%; (d) 30%; (e) 40%

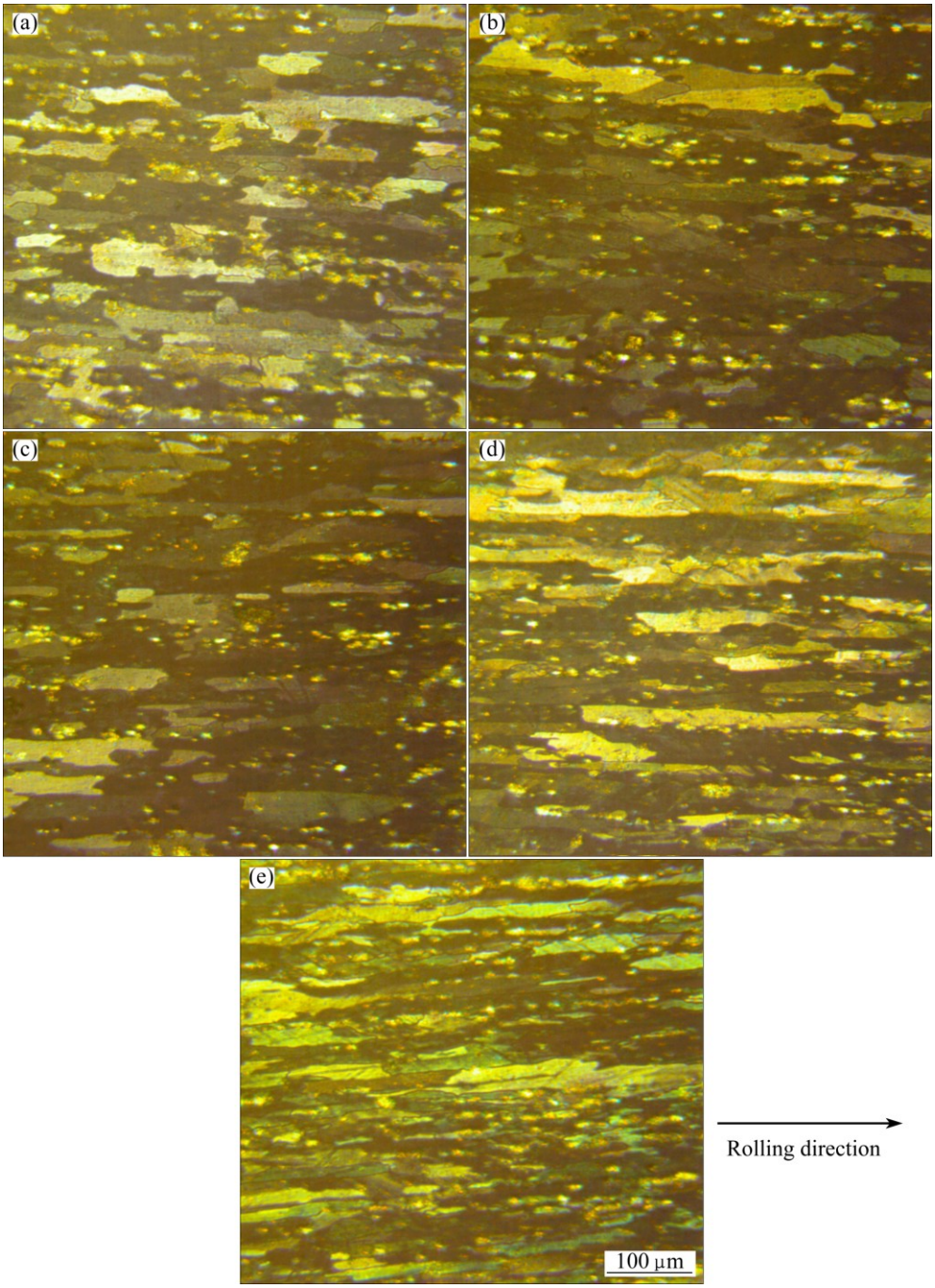

Fig. 4 Optical micrpgraphs of peak-aged samples at different ε_r: (a) 0; (b) 10%; (c) 20%; (d) 30%; (e) 40%

Meanwhile, large particles at the grain boundaries and coarse second phase in the grain interior are presented in Fig. 4 (as shown by arrows). Referring to the higher deformation level (40%) shown in Fig. 4(e), the grains are compressed to more flat and elongated, and the second phases are arrayed along the RD, resulting in fiber structures. It is apparent that grain sizes are decreased and thickness of grains reduces with increasing pre-strain, and the grain size of sample with ε_r=40% is the smallest compared with other alloys.

The microstructure of the SST+CR samples was examined in more detail using TEM. Bright-field (BF) TEM images along a zone axis close to $[001]_{Al}$ and corresponding selected area diffraction (SAD) patterns are presented in Fig. 5. There are no detectable precipitate and an extremely low dislocation density in as-quenched alloy (Fig. 5(a)), meanwhile, only diffraction from Al is observed in the inset SAD in Fig. 5(a), suggesting that no secondary phase forms in this sample. In contrast, from Figs. 5(b) and (c), a large number of dislocations are generated due to CR, indicating typical BF TEM micrographs of an as-rolled

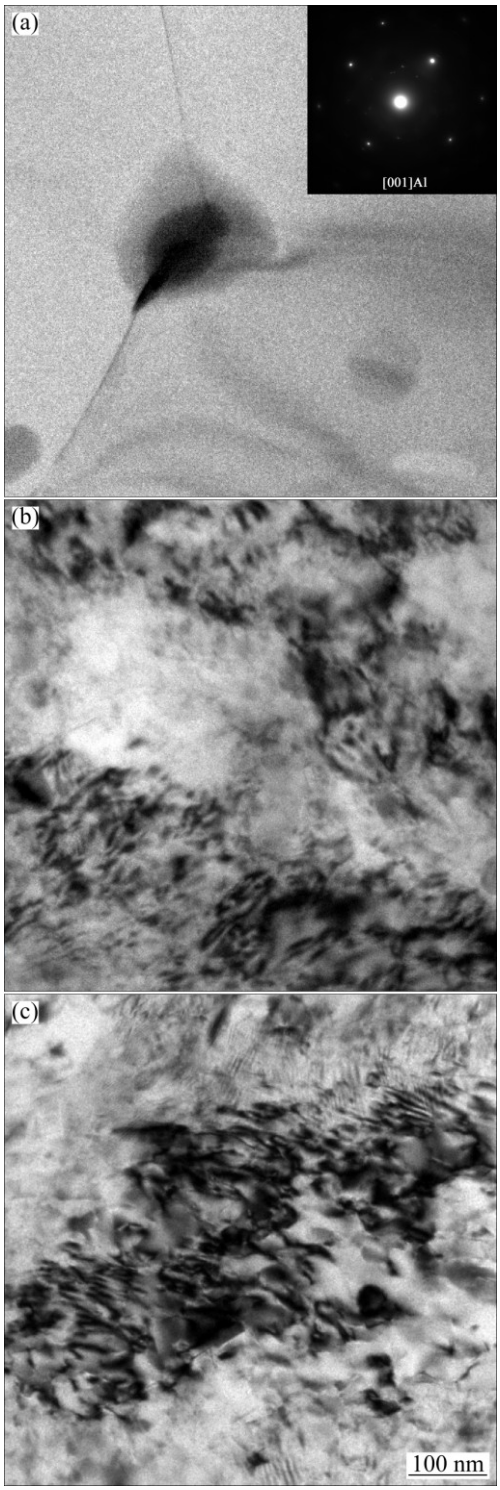

Fig. 5 $\langle 001\rangle_{\alpha}$ BF TEM images of alloys with various strains: (a) 0; (b) 20%; (c) 40% (Inset in (a) is the corresponding SAD pattern recorded along $\langle 001\rangle$)

sample. The density of dislocation keeps increasing with rolling strain. Figure 5(c) contains the highest density of dislocations, which is responding to the initial hardness in the hardness curves in Fig. 1. Hardness increase is caused by work-hardening that generates many tangled dislocations.

The TEM and high-resolution TEM (HRTEM) images for samples in their peak-aged conditions are presented in Fig. 6. As illustrated in these figures, recovery has occurred due to the aging, and thickness of the dense dislocation walls is reduced, indicating a dramatic decrease in dislocation density. Main strengthening phase of the alloys used in present work with Cu-to-Mg mass ratio equal to 3.2:1 is S' (Al_2CuMg). The precipitation sequence of this alloy [18−20] is SSS→GP I zone→GP II zone→S'→S, where SSS stands for supersaturated solid solution. The S' phase is believed to preferentially precipitate on dislocations [21]. Needle-shaped nanometer-sized precipitates can be clearly observed by tilting the specimens close to the $\langle 001\rangle_{Al}$ zone axis (Figs. 6(f) and (g)). As shown in Fig. 6, the density of dislocation keeps increasing with rolling strain. Thus, the S' precipitates become more closely spaced and thinner after pre-aging deformation. As shown in Fig. 6(a), the sample with ε_r=10% undergoes obvious recovery, and a small amount of nanometer-sized S' precipitates appear. The precipitation thickness is too thin to be determined accurately from the image; however, the presence of S' precipitates can be determined from the streaking of the precipitate diffraction spots. By contrast, the amount of S' precipitate is slightly increased in the sample with ε_r=20% (Fig. 6(f)). These needle-like S' precipitates are distributed heterogeneously in the grain volume. Both the density and the amount of S' precipitate are increased when rolling strain ranges from 10% to 40%. Figures 6(b) and (d) show the corresponding HRTEM images confirming the formation of sub-nanometer thick S' precipitates in the samples with ε_r=10% and 20% in their peak-aged conditions, respectively. The length of those precipitates is only several nanometers, according to the HRTEM observation. Similar microstructure and SAD pattern were also obtained by ZHAO et al [15] in Al 2024 alloy through the combination of SST, CR and artificial aging.

4 Discussion

4.1 Factors affecting strength

It is apparent from Fig. 1 that the aging time to achieve peak hardness is reduced after performing CR on SST samples. Firstly, since dislocation density increases drastically during CR, which provides heterogeneous nucleation sites for precipitates, reducing the total time for precipitation. Secondly, it is expected that pre-strain enhances diffusion rates of Cu and Mg through dislocation pipes, resulting in a finer distribution and smaller size of precipitates than that of the SST samples (Fig. 6). CHEN et al [22] suggested that pre-strain before peak aging results in acceleration of overall precipitation

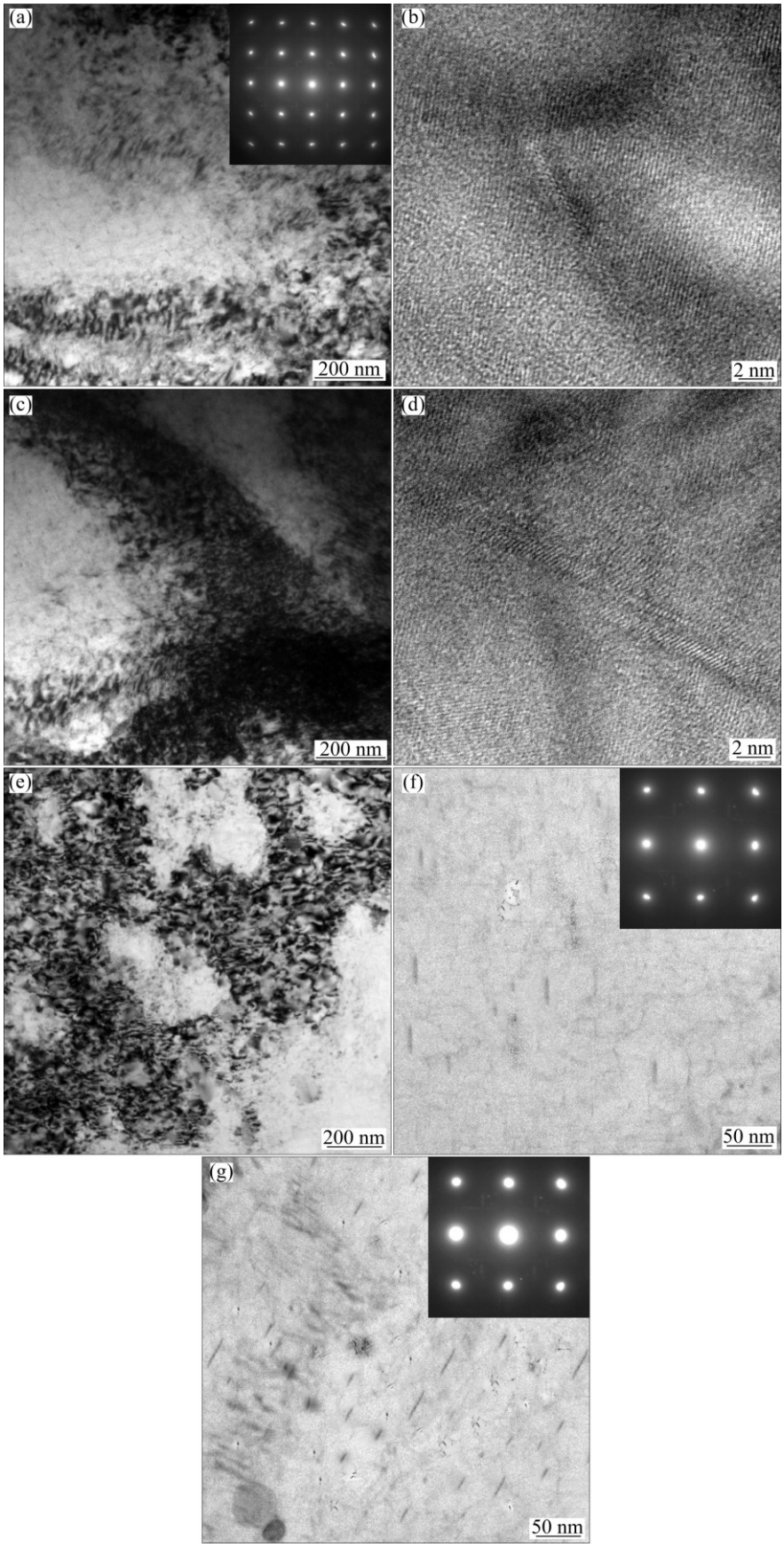

Fig. 6 TEM and HRTEM images of peak aging samples with different pre-deformation: (a, b) 10%; (c, d, f) 20%; (e, g) 40% (Upper right insets in (a), (f) and (g) are corresponding SAD patterns. (f) and (g) are TEM images recorded along zone axis close to $[001]_{Al}$ to show *S′* precipitates)

kinetics and increasing peak hardness with increasing strain. The same conclusion can be drawn for the current case from the above discussion.

As shown in Fig. 2(a), the YS and UTS of the as-rolled samples are much higher than those of the T6 material. This increase in strength is attributed to fine precipitates, high density of dislocations and small grain size [23]. The strength of the material depends on the interaction of the second phase particles and mobile dislocations. Fine precipitate phase increases the strength of the rolled samples, due to the Orowan strengthening mechanism [24,25]. Aside from this, a large number of dislocations are another main source of strengthening for the CR alloy by work- hardening mechanism. These dislocations interacted with one another and also with the precipitates, leading to higher strength and hardness of the samples. In addition, the dislocations can provide nucleation sites for the precipitation phases [26]. Therefore, the number density of S' phases in CR alloy is larger than that of the non-deformed alloy (Figs. 5 and 6). Furthermore, grain refinement also plays a positive role in the strengthening of the samples. Figure 4 shows that grain size of the rolled samples is slightly smaller than that of the T6 material and it decreases with increasing strain according to the Hall−Petch equation, [24,27].

As shown in Fig. 2, the UTS of the sample with ε_r=40% is 531.4 MPa, which is higher by ~100 MPa than that of non-deformed sample (431.2 MPa). This increase was caused by the high density of S' precipitates generated during the aging. During the aging, the following changes in microstructures occurred (Fig. 6). Firstly, the high density of dislocations introduced by CR decreases via recovery, which impairs the effect of work-hardening, resulting in decreasing the strength of the SST + CR sample. Secondly, the growth of grains eliminated most of the strengthening effect by grain refinement. Thirdly, a large number of nano-sized S' precipitates were formed. Obviously, the contribution to strength from nano-sized S' precipitates not only compensated for the strength decrease caused by the grain growth and dislocation density decrease, but also further increased the UTS by ~100 MPa, attributing to the effectiveness of a high density of S' precipitates in enhancing the strength [11,28−30]. Precipitation strengthening depends on an effective interparticle spacing, L', i.e., $\tau_p \propto 1/L'$ [31] ($L'=r/f$, where r is the average diameter of precipitates and f is the volume fraction of precipitations). Thus, the strength increase due to precipitation can be written as

$$\sigma_p = k\frac{f}{r} \quad (1)$$

Obviously, for a fixed f, an increase of nucleation sites would decrease the precipitate particle size r, hence, the age hardening would be more effective [28]. Compared with the other two samples subjected to lower rolling strain (Figs. 6(a) and (f)), the sample with ε_r=40% aged for 175 min has smaller and higher density of S' precipitates (Fig. 6(g)), which are effective in impeding dislocation motion, thus, leading to higher strength than that of the sample with ε_r=20% aged for 225 min (peak-aged condition).

4.2 Factors affecting ductility

Although the UTS of the sample with ε_r=40% is higher by ~100 MPa than that of sample without pre-strain, its El falls to ~9.9%. Strain hardening is known to have an adverse effect on the ductility. During CR, the alloy undergoes large plastic deformation and therefore the dislocation density increases significantly (Fig. 5), these dislocation tangles make difficulty for its movement, decreasing the ductility of the alloy. In addition, by performing aging after rolling, the following changes in microstructures take place. The precipitation formed during aging. S' precipitates were found to be effective in pinning dislocation and resisting gliding of dislocation, which impair the ability of further plastic deformation through dislocation accumulation, resulting in poor ductility of the alloy. Furthermore, a high density of ultrafine S' precipitates should increase the strain concentration to some extent. The dislocation density introduced by rolling is decreased via recovery, which will increase elongation. The grain growth during aging should improve the ductility. Grain coarsening or/and relaxation of internal stresses during aging has been considered to cause the ductility increase [11]. It is likely that this improvement is not enough to compensate for the decrease in ductility caused by ultrafine S' precipitates [32].

5 Conclusions

1) Pre-deformation by cold rolling is effective in increasing the strength of Al−Cu−Mg alloy. The sample with ε_r=40%, the YS and UTS of 446.1 and 531.4 MPa are achieved, respectively, while maintaining a good El of 9.9%.

2) Double-peak age strengthening was achieved in CR-processed high purity Al−Cu−Mg alloy upon aging at 453 K.

3) Pre-deformation can result in a higher hardness compared with conventional T6 heat-treated high purity Al−Cu−Mg alloy, and it can reduce the time to reach peak hardness.

4) The strengthening mechanisms for age strengthening peak of the CR-processed samples are the enhanced particle density and finer S' distribution besides the strain hardening and grain refinement.

References

[1] STYLES M J, MARCEAU R K W, BASTOW T J, BRAND H E A, GIBSON M A, HUTCHINSON C R. The competition between metastable and equilibrium *S*(Al_2CuMg) phase during the decomposition of Al−Cu−Mg alloys [J]. Acta Materialia, 2015, 98: 64−80.

[2] WANG S C, STARINK M J. Precipitates and intermetallic phases in precipitation hardening Al−Cu−Mg−(Li) based alloys [J]. International Materials Reviews, 2005, 50: 193−215.

[3] WANG S C, STARINK M J. Two types of *S* phase precipitates in Al−Cu−Mg alloys [J]. Acta Materialia, 2007, 55: 933−941.

[4] AFZAL N, SHAH T, AHMAD R. Microstructural features and mechanical properties of artificially aged AA2024 [J]. Strength of Materials, 2013, 45(6): 684−692.

[5] RADMILOVIC V, KILLAS R, DAHNEN U, SHIFLET G J. Structure and morphology of *S*-phase precipitates in aluminum [J]. Acta Materialia, 1999, 47: 3987−3997.

[6] ABIS S, MASSAZZA M, MENGUCCI P, RIONTINO G. Early aging mechanisms in a high-copper AlCuMg alloy [J]. Scripta Materialia, 2001, 45: 685−691.

[7] POPOV N N, PROKOSHKIN S D, SIDORKIN M YU, SYSOEVA T I, BOROVKOV D V, AUSHEV A A, KOSTYLEV I V, GUSAROV A E. Effect of thermomechanical treatment on the structure and functional properties of a 45Ti−45Ni−10Nb alloy [J]. Russian Metallurgy, 2007, 1: 59−64.

[8] WEI Xiu-yu, ZHENG Zi-qiao, PAN Zheng-rong, CHEN Yuan-yuan, LI Shi-chen, CHEN Qiu-ni. The role of plastic deformation on microstructure and mechanical properties of 2197 Al−Li alloy [J]. Rare Metal Materials and Engineering, 2008, 37: 1996−1999.

[9] QUAN Li-wei, ZHAO Gang, Sam GAO, Barry C. MUDDLE. Effect of pre-stretching on microstructure of aged 2524 aluminium alloy [J]. Transactions of Nonferrous Metals Society of China, 2011, 21(9): 1957−1962.

[10] NING Ai-lin, LIU Zhi-yi, ZENG Su-min. Effect of large cold deformation on characteristics of age-strengthening of 2024 aluminum alloys [J]. Transactions of Nonferrous Metals Society of China, 2006, 16(5): 1121−1128.

[11] HUANG Yu-jin, CHEN Zhi-yong, ZHENG Zi-qiao. A conventional thermo-mechanical process of Al−Cu−Mg alloy for increasing ductility while maintaining high strength [J]. Scripta Materialia, 2011, 64: 382−385.

[12] ÜNLÜ N, GABLE B M, SHIFLET G J, STARKE E A Jr. The effect of cold work on the precipitation of Ω and θ' in a ternary Al−Cu−Mg alloy [J]. Metallurgical and Materials Transactions A, 2003, 34: 2757−2769.

[13] LI Zhou-bing, SHEN Jian, LEI Wen-ping, YAN Liang-ming, LI Peng, MAO Bai-ping. Effects of prestretching on precipitated phase and mechanical properties of Al−Cu−Mg−Ag alloy [J]. The Chinese Journal of Nonferrous Metals, 2010, 20(8): 1508−1512. (in Chinese)

[14] RINGER S P, MUDDLE B C, POLMEAR I J. Effects of cold work on precipitation in Al−Cu−Mg−Ag and Al−Cu−Li−Mg−Ag alloys [J]. Metallurgical and Materials Transactions A, 1995, 26: 1659−1671.

[15] ZHAO Yun-long, YANG Zhi-qing, ZHANG Zhen, SU Guo-yue, MA Xiu-liang. Double-peak age strengthening of cold-worked 2024 aluminum alloy [J]. Acta Materialia, 2013, 61: 1624−1638.

[16] REN Jie-ke, CHEN Zhi-guo, HUANG Yu-jin, ZHANG Ji-shuai, WEI Xiang, FANG Liang. Effect of new thermo-mechanical treatment on microstructure and properties of 2E12 aluminum alloy [J]. The Chinese Journal of Nonferrous Metals, 2014, 24(3): 643−650. (in Chinese)

[17] HORITA Z, FUJINAMI T, NEMOTO M, LANGDON T G. Improvement of mechanical properties for Al alloys using equal-channel angular pressing [J]. Journal of Materials Processing Technology, 2001, 117: 288−292.

[18] VIALA J C, BOSSELET F, LAURENT V, LEPETICORPS Y. Mechanism and kinetics of the chemical interaction between liquid aluminum and silicon−carbide single crystals [J]. Journal of Materials Science, 1993, 28: 5301−5312.

[19] SANNINO A P, RACK H J. Effect of reinforcement size on age hardening of PM 2009 Al−SiC 20vol% participate composites [J]. Journal of Materials Science, 1995, 30: 4316−4322.

[20] CAROTEWIO G, GALLO A, NICOWS L. Degradation of SiC particles in aluminium-based composites [J]. Journal of Materials Science, 1994, 29: 4967−4974.

[21] RADMILOVIC V, THOMAS G, SHIFTER G J, STARKE JR E A. On the nucleation and growth of Al_2CuMg (*S'*) in AlLiCuMg and AlCuMg alloys [J]. Scripta Materialia, 1989, 23: 1141−1146.

[22] CHEN Yu-te, LEE Sheng-long, BOR Hui-yun, LIN Jing-chie. Effect of natural aging and cold working on microstructures and mechanical properties of Al−4.6Cu−0.5Mg−0.5Ag alloy [J]. Metallurgical and Materials Transactions A, 2013, 44: 2831−2838.

[23] MIRZAEI M, ROSHAN M R, JENABALI JAHROMI S A. Microstructure and mechanical properties relation in cold rolled Al 2024 alloy determined by X-ray line profile analysis [J]. Materials Science and Engineering A, 2015, 620: 44−49.

[24] ROSHAN M R, MIRZAEI M, JENABALI JAHROMI S A. Microstructural characteristics and tensile properties of nano-composite Al 2014/4 wt.% Al_2O_3 produced from machining chips [J]. Journal of Alloys and Compounds, 2013, 569: 111−117.

[25] IBRAHIM I A, MOHAMED F A, LAVERNIA E J. Particulate reinforced metal matrix composites — A review [J]. Journal of Materials Science, 1991, 26: 1137−1156.

[26] AN Li-hui, CAI Yang, LIU Wei, YUAN Shi-jian, ZHU Shi-qiang, MENG Fan-cheng. Effect of pre-deformation on microstructure and mechanical properties of 2219 aluminum alloy sheet by thermomechanical treatment [J]. Transactions of Nonferrous Metals Society of China, 2012, 22(S2): s370−s375.

[27] HALL E O. The deformation and aging of mild steel: III. Discussion of results [J]. Proceedings of the Physical Society B, 1951, 64: 747−752.

[28] CHENG S, ZHAO Y H, ZHU Y T, EVAN M A. Optimizing the strength and ductility of fine structured 2024 Al alloy by nano-precipitation [J]. Acta Materialia, 2007, 55: 5822−5832.

[29] KIM W J, CHUNG C S, MA D S, HONG S I, KIM H K. Optimization of strength and ductility of 2024 Al by equal channel angular pressing (ECAP) and post-ECAP aging [J]. Scripta Materialia, 2003, 49: 333−338.

[30] ZHENG Rui-xiao, SUN Yan-bo, AMEYAMA Kei, MA Chao-li. Optimizing the strength and ductility of spark plasma sintered Al 2024 alloy by conventional thermo-mechanical treatment [J]. Materials Science and Engineering A, 2014, 590: 147−152.

[31] COURTNEY T H. Mechanical behavior of materials [M]. New York: McGraw-Hill, 1990.

[32] WANG Z C, PRANGNELL P B. Microstructure refinement and mechanical properties of severely deformed Al−Mg−Li alloys [J]. Materials Science and Engineering A, 2002, 328: 87−97.

预变形对高纯 Al−Cu−Mg 合金组织和力学性能的影响

李慧中[1,2,3]，刘若梅[1]，梁霄鹏[1,2]，邓 敏[1]，廖慧娟[1]，黄 岚[2]

1. 中南大学 材料科学与工程学院，长沙 410083；
2. 中南大学 粉末冶金国家重点实验室，长沙 410083；
3. 中南大学 有色金属材料科学与工程教育部重点实验室，长沙 410083

摘 要：通过拉伸测试、硬度测试、扫描电镜以及透射电镜等手段，研究预变形对高纯 Al−Cu−Mg 合金 180 °C 时效后组织和力学性能的影响。结果表明：与未预变形的样品相比，随着预轧制量的增加，预轧制后样品的峰值硬度值逐渐增加，而达到峰值硬度所需的时间也逐渐缩短。此外，在预变形的合金时效过程中观察到双峰硬化现象。TEM 的研究结果表明，经冷轧变形的合金随着预变形量的提高，合金中 *S*′(Al_2CuMg)相的密度增大，尺寸减小，这种高密度、细小的 *S*′相以及高密度位错是导致合金峰值硬度和强度提高的主要原因。

关键词：Al−Cu−Mg 合金；预变形；人工时效；析出相；显微组织；力学性能

(Edited by Xiang-qun LI)